A Refreshable Braille Cell Based on Pneumatic Microbubble Actuators

Xiaosong Wu, Seong-Hyok Kim, Haihong Zhu, Chang-Hyeon Ji, and Mark G. Allen, *Fellow, IEEE*

***Abstract*—A refreshable Braille cell as a tactile display prototype has been developed based on a 2 × 3 pneumatic microbubble actuator array and an array of commercial valves. The microbubble actuator acting as a Braille dot consists of a parylene corrugated diaphragm and an overcoated elastomer layer. Polyurethane (PU) and polydimethylsiloxane (PDMS) elastomer-based Braille cells were fabricated and compared in terms of their displacement–pressure characteristics, force–displacement characteristics, dynamic response, and hysteresis of elastic deformation. Both PU- and PDMS-based pneumatic Braille cells demonstrate satisfactory properties against the static and vibrational tactile display requirements. The displacement of the PU-based Braille dot is 0.56 mm at a 0.2-Hz operating frequency, and the generated force is 66 mN at a 100-kPa applied pressure. The strong hysteresis observed in microbubble actuators made with PU elastomer is resolved by the use of PDMS elastomer. The refreshable Braille cell was also designed to meet the criteria of lightness and compactness to permit portable operation. The design is scalable with respect to the number of tactile actuators while maintaining fabrication simplicity. [2011-0104]**

***Index Terms*—Braille, pneumatic actuators, polymer films, soft lithography, stereolithography.**

I. Introduction

TACTILE DISPLAYS, which convey information by stimulating the sense of touch, rely on actuators to generate spatial resolution in terms of three-dimensional (3-D) structure and movement. A simple example of a tactile display is a refreshable Braille display (RBD) that converts electronic text information from a computer to Braille dots for the visually impaired to read [1]. Tactile displays have other important applications in areas such as virtual reality [2], teleoperation and telepresence [3], vision–tactile substitution [4], fundamental haptic science research [5], video games, online shopping, and mediated social touch. Advanced tactile displays had not been widely available, primarily due to the lack of low-cost large-area compact actuator arrays that can stimulate a large number of receptors on the user and that can also meet the high requirements for user safety and comfort.

Manuscript received April 11, 2011; revised December 28, 2011; accepted January 6, 2012. Date of publication April 12, 2012; date of current version July 27, 2012. This work was supported in part by the National Science Foundation "Digital Clay" project under Contract IIS-0121663. Subject Editor C. H. Ahn.

X. Wu is with The Dow Chemical Company, Midland, MI 48674 USA (e-mail: xswu@dow.com).

S.-H. Kim, H. Zhu, and M. G. Allen are with the Georgia Institute of Technology, Atlanta, GA 30332 USA (e-mail: seonghyok.kim@gmail.com; zhu.hhong@gmail.com; mark.allen@ece.gatech.edu).

C.-H. Ji is with the Department of Electronics Engineering, Ewha Womans University, Seoul 120-750, Korea (e-mail: cji@ewha.ac.kr).

Color versions of one or more of the figures in this paper are available online at http://ieeexplore.ieee.org.

Digital Object Identifier 10.1109/JMEMS.2012.2190043

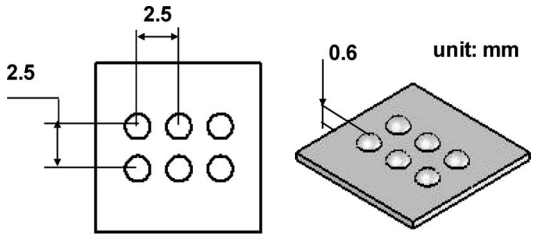

Fig. 1. International building standard for a Braille cell.

An RBD device can be built, for example, according to the international Braille building standard shown in Fig. 1 [1], [6]. Almost all available actuation technologies have been investigated for RBD and vibratory tactile displays. Examples of microactuators that have been used include electromagnetic [7], piezoelectric [8], shape memory alloy [9], [10], electroactive polymer [11], thermopneumatic [12], and surface acoustic wave actuators [13]. However, there are defects associated with each actuation technology. Such defects include, for example, insufficient force, insufficient stroke, and/or slow response time.

In order to develop a portable and multiline RBD, a mass-manufacturable, lightweight, low-power, and integrable actuator is needed. Several research groups have turned to microelectromechanical systems (MEMS) technology and fabricated different types of tactile displays. Lee *et al.* reported an electrothermal RBD that required 50 s to raise and retrieve a dot, but force data were not available [1]. Kato *et al.* reported a 6 × 4 array of sheet-type RBD based on an ionic polymer metal composite actuator that had a maximum displacement of 0.4 mm and 1.5-gf (∼14.7 mN) generated force. But this fabricated device still required 0.9 s to reach a 0.2-mm displacement [14]. A recently reported thermopneumatic tactile display had an actuator array consisting of a flexible diaphragm and a bottom plate bonded together to create a cavity between them. A microneedle and a microheater were formed on the diaphragm, and the sealed cavity was prefilled with a liquid. These components were manually assembled to form a 3 × 3 arrayed actuator device with a dimension of $15 \times 15 \times 1$ mm^3. The device had a needle displacement of 61 μm with 457-mJ input energy [15].

Pneumatic actuation is a promising candidate for Braille cell actuation by virtue of its rapid response time and potential for large-force generation while maintaining simplicity, scalability, and low cost. A valve for an elastic membrane-type pneumatic RBD was demonstrated by Yobas *et al.* [16]. In the pneumatic

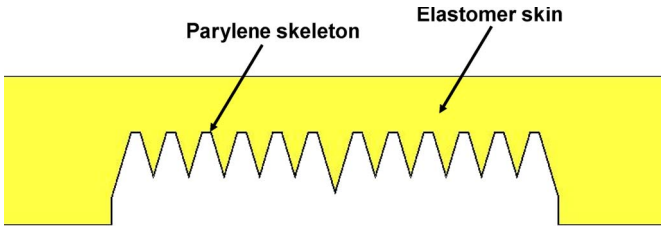

Fig. 2. Cross-sectional schematic of an endoskeletal microbubble actuator.

tactile display, the deforming elastomer membrane amplifies the microvalve's actuation, thereby increasing the tactile acuity of the display. At the same time, the membrane acts as a "tactile screen" to protect the microvalves against the excessive downward force of the user. In their work, the elastomeric membrane was actuated under a pressure load of 27.6 kPa. However, pneumatic actuators are balloon-shaped and made of planar isotropic membrane. They typically deflect omnidirectionally into a spherical shape, which makes them undesirable for indentation type of tactile display applications that require more directional or linear movements. Furthermore, the relationship between actuation pressure and radius of inflation may not be monotonic in all pressure ranges, raising instability issues under widely varying external loads [17]. When the external load varies from several tens of millinewtons (when the finger is actively touching the tactor) to zero (when the finger is lifted), the balloon actuator may hyperinflate when the load is low or zero.

As an alternative, an endoskeletal microbubble actuator capable of reversible vertical deflection was developed [18]. The microbubble actuator has a kinematic stabilization design through combining two polymeric layers with complementary functions, as shown in Fig. 2. The microcorrugated parylene diaphragm layer acts as a "skeleton" to provide directional deflection in a desired axial direction while suppressing undesired lateral deflections; an overcoated polyurethane (PU) elastomer layer acts as a "skin" to help the extended membrane recoil to its original shape, ensuring diaphragm stability. In a later study, a refreshable Braille cell was developed based on a 2×3 endoskeletal microbubble array by further reducing the diameter of the actuator from 3 mm to 1.5 mm, optimizing the corrugated-diaphragm design, and increasing the spatial density of the microbubble actuator [6]. A displacement of 0.56 mm at a 0.2-Hz operating frequency and a 66-mN force at a 100-kPa applied pressure were achieved. The aim of the currently reported work, which is an extension and expansion of the work described in [6], was to characterize the critical properties of the Braille display, including force generation, mechanical bandwidth, pneumatic power consumption, and lifetime against the requirements for both static and vibrational tactile displays. Also provided in this paper is design guidance based on the theoretical correlation between the actuator displacement and the thickness of the parylene diaphragm and of the PU layer. Furthermore, an alternative elastomer has been evaluated in this paper to resolve the strong hysteresis of PU-based microbubble actuators. A polydimethylsiloxane (PDMS)-based Braille cell was fabricated and compared with a PU-based Braille cell in terms of the critical performance characteristics as a tactile display as well as the hysteresis of elastic deformation.

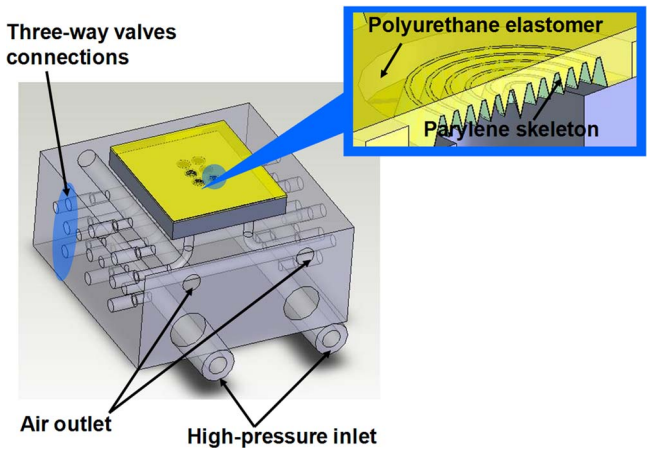

Fig. 3. Schematic of the laminated pneumatic actuator layer on the fluidic manifold.

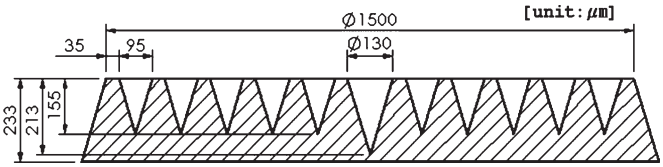

Fig. 4. Profile and dimensions of the designed corrugated diaphragm [6].

II. Design

A. Braille Cell

The proposed Braille cell consists of three components: a pneumatic actuator layer, a fluidic manifold, and valves and electronics. A schematic of the Braille cell without externally assembled valves and electronics is shown in Fig. 3. Six three-port valve connections, two high-pressure inlets, and two air outlets are incorporated into the manifold. The Braille cell is operated under regulated compressed air. The on-and-off of a Braille dot is controlled by a miniature solenoid valve attached to the three ports on the side of the manifold. For each solenoid valve, the middle port is the common port and links to the actuator, the lower port links to the high-pressure inlet, and the upper port links to the exhaust channel (air outlet channel). When the solenoid valve is not powered, the actuator is linked to the exhaust channel through the upper port, which is a normally open port; when the valve is powered, the exhaustion is closed, and the air inlet is open to allow compressed air to flow into the microbubble actuator through the lower port.

B. Pneumatic Actuator

The pneumatic actuator layer is constructed with six endoskeletal microbubble actuators arranged in a 2×3 array on a stereolithography (SLA) substrate. The design of the endoskeletal microbubble actuator has been reported in [6]. Because displacement more than 0.6 mm is not typically required for a Braille cell, the bubble stability can be enhanced by reducing the actuator displacement through decreasing the depth of the second corrugation from the center from that of the previous design in [18]. A schematic view and the dimensions of the designed corrugated diaphragm are shown in Fig. 4.

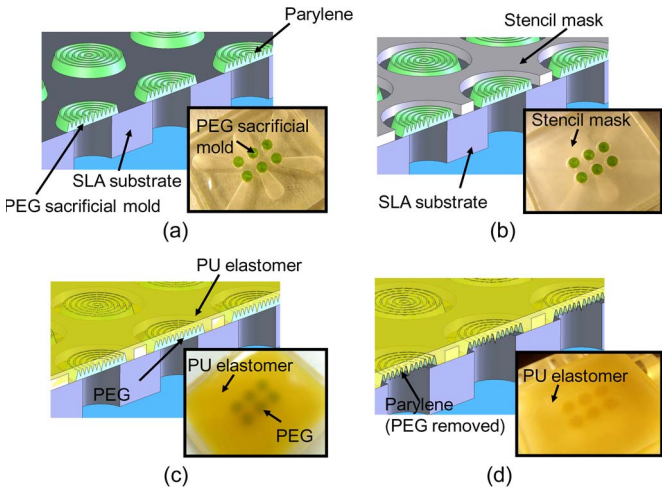

Fig. 5. Fabrication process steps. (a) PEG micro transfer molding and parylene coating. (b) Planarization with SLA stencil mask. (c) PU coating and curing. (d) Removal of PEG sacrificial mold.

III. Fabrication Process

An array of the original mold of a corrugated diaphragm was fabricated by inclined rotational UV lithography. The sacrificial polyethylene glycol (PEG) mold was transfer-molded onto an SLA substrate with open orifices that connect to the fluidic manifold. Detailed fabrication processes for the PEG corrugated-diaphragm molds are described elsewhere [6], [18].

The PEG mold array was transfer-molded on the SLA substrate, and a thin parylene-C layer was conformally deposited on the PEG mold array [Fig. 5(a)]. An epoxy stencil mask was placed on the SLA substrate to planarize the top surface [Fig. 5(b)]. After that, a two-component room-temperature-vulcanizing liquid PU elastomer (Poly 74-20, PolyTek) was spin-coated on the top and cured at room temperature for 48 h [Fig. 5(c)]. The PEG mold was then removed in water [Fig. 5(d)]. This fabrication process is mass-manufacturing compatible. Large arrays of Braille cells can be fabricated without additional steps.

After the SLA substrate was assembled, a thin PDMS prepolymer was applied as bonding adhesive to the contact surface between the SLA substrate and an SLA manifold and was allowed to cure for 24 h at room temperature before the subsequent assembly and testing. The SLA substrate with microbubble actuator array was thus bonded by cured PDMS to the SLA manifold, which pneumatically addresses each microbubble, as shown in Fig. 6(a). Finally, six three-way solenoid valves were connected to the manifold to control the individual actuators. The assembled device is shown in Fig. 6(b). The fully assembled device measures 56 mm $\times$ 61 mm $\times$ 52 mm ($L \times W \times H$) and weighs 91 g.

IV. Results and Discussion

The performance of the RBD device was assessed from the following perspectives: spatial resolution, displacement, force generated, mechanical bandwidth, pneumatic power consumption, and lifetime.

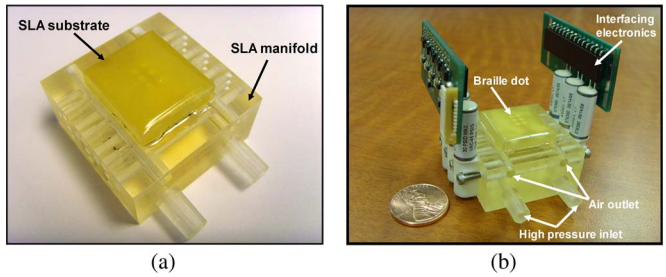

Fig. 6. Assembly of the actuator layer to manifold and microvalves. (a) Bonded actuator layer and manifold. (b) Final assembled device with microvalves.

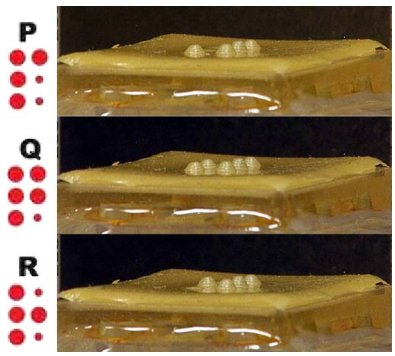

Fig. 7. Actuation of Braille dots corresponding to Braille alphabets.

A. Spatial Resolution

It is generally accepted that the spatial resolution of actuators should be approximately 1 actuator/mm^2 [19]. An array of tactile actuators packed denser than the spatial acuity would lead to a continuous tactile sensation at the fingertip, which is not favorable in the Braille display application. In Fig. 7, Braille dots were selectively actuated to represent the characters "P," "Q," and "R" in American Braille style. The center-to-center distance between two adjacent dots was measured by a moving-stage microscopy as 2.5 mm, which exceeds the minimum discernable distance of 2 mm on a fingertip [20].

B. Displacement

Optical microscopic photographs of a Braille dot in its inactuated and actuated states are shown in Fig. 8. Large deflection is achieved preferentially in the vertical direction, which makes the shape more distinguishable than the hemispherical shape of a pure elastomer balloon actuator. The center displacement of a Braille dot (in this case, the microbubble actuator) as a function of applied pressure has been quantitatively characterized using a laser displacement sensor. At an actuation frequency (i.e., valves turned on and off) of 0.2 Hz, the maximum, minimum, and peak-to-peak displacements of the Braille dot were measured at each level of applied pressure. This frequency, i.e., a refresh rate of 1 letter/5 second, is sufficient for a 50-cell refreshable Braille display, assuming a Braille reading speed of 124 words/minute [21] (about 10 letters/second).

A finite-element analysis was performed for the Braille dot using the ANSYS finite-element program. Two ANSYS element types were used in the simulation: plane 82 for parylene

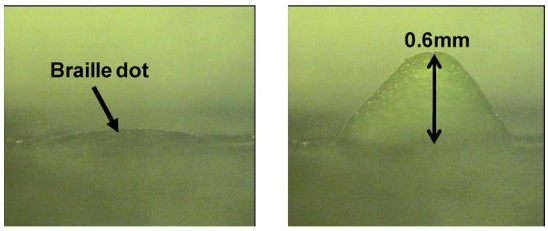

Fig. 8. Microscopic images of the inactuated and the actuated Braille dot. (a) Inactuated Braille dot. (b) Actuated dot at 100 kPa.

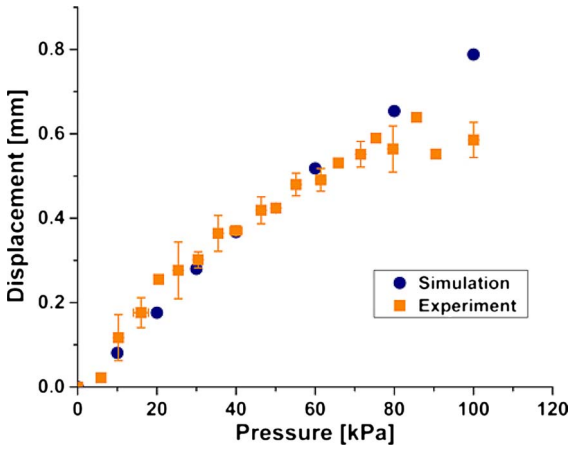

Fig. 9. FEM and experimental results of averaged dot heights for a PU Braille cell.

and hyper 84 for PU elastomer. Plane 82 is a 2-D eight-node structural solid element with large-strain capability, and hyper 84 is a hyperelastic solid element based on the Mooney–Rivlin nonlinear elastic model [18]. The Mooney–Rivlin constants used in the ANSYS simulation were derived from the stress–strain curve obtained by a uniaxial tensile test. The center displacement of one Braille dot as a function of applied pressure was determined from the simulation. Fig. 9 compares the finite-element modeling (FEM) and the experimental results for a microbubble actuator with 2.5-μm-thick parylene and 100-μm-thick PU. As shown in Fig. 9, the simulation results (represented by circles) are in excellent agreement with the experimental results (represented by the squares) up to a 70-kPa applied pressure. Starting from a pressure load of 79 kPa, the directional stability of the microbubble actuator decreases, because at this point, the maximum displacement of the microbubble actuator is shifted from the vertical center and the shape of the microbubble actuator loses its symmetry.

PU elastomer has been used to fabricate micro-/nanostructures for various MEMS applications [22]. In our work, it was selected to form the elastic overcoating layer for the Braille dot due to its superior mechanical robustness such as high tear and abrasive resistances, excellent chemical and grease resistance, and low gas permeability, all of which are important to a pneumatic Braille display. However, the PU-based microbubble actuator demonstrated relatively large hysteresis of elastic deformation during inflation and deflation cycles [18]. PUs are copolymers consisting of soft and hard segments, and the permanent deformation of the latter is believed to cause large hysteresis [23]. A potential alternative

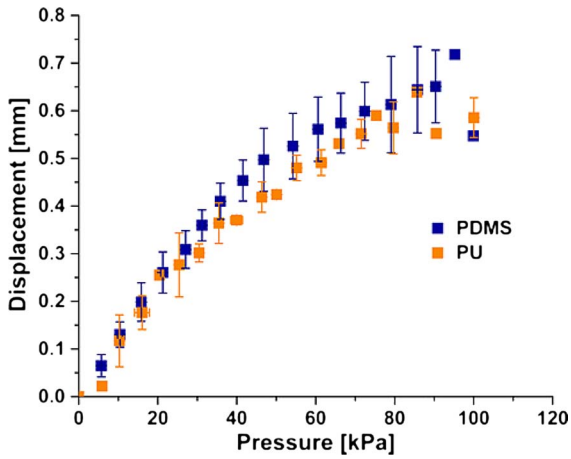

Fig. 10. Averaged dot heights for a PDMS Braille cell and a PU Braille cell as a function of applied pressure.

elastomer candidate for the overcoat layer is PDMS, an elastomer that has been widely used in MEMS applications. The low-viscosity and room-temperature curing feature of PDMS made it suitable as a replacement for PU in this application. It was hypothesized that PDMS would have a lower hysteresis due to the absence of domain structure of hard and soft segments. It was the aim of this paper to compare the key properties of a PDMS- and a PU-based Braille cell. The averaged maximum displacements of three PU-based Braille dots with 2.5-μm-thick parylene and 100-μm-thick PU and those of three PDMS-based Braille dots with 2.5-μm-thick parylene and 50-μm-thick PDMS are shown in Fig. 10. Because the 100% modulus of PDMS was measured to be 0.65 MPa, about two times higher than that of PU elastomer (0.3 MPa), the thickness of the PDMS layer was 50 μm in a PDMS-based Braille cell, half of that of the PU layer. A comparable displacement response was achieved for a PDMS-based Braille cell.

C. Force Generated

Each Braille dot needs to withstand at least 50-mN contact force while maintaining at least 0.25-mm displacement in order to stimulate the shallowest mechanoreceptor [24]. The force generated by a single Braille dot as a function of displacement has been characterized. The force at various displacements was determined by the experimental procedure shown in Fig. 11. First, a Braille cell was placed on a scale with an accuracy of 0.1 g. A small piston was mounted on a readable moving z stage. Under a constant applied pressure, the piston was brought down to touch the inflated microbubble actuator at a "zero-force" position, where the bubble actuator maintained its maximum displacement. The piston was then moved downward at a fixed interval while a constant pressure was being supplied to the microbubble actuator. The reaction force was read from the scale. This procedure was repeated for a range of displacements and pressures.

The results for a PU Braille dot at 66 and 100 kPa are compared with the results for a PDMS Braille dot at 66 kPa in Fig. 12.

For each static applied pressure, the force-versus-displacement curve is shown in Fig. 12. The slope of the

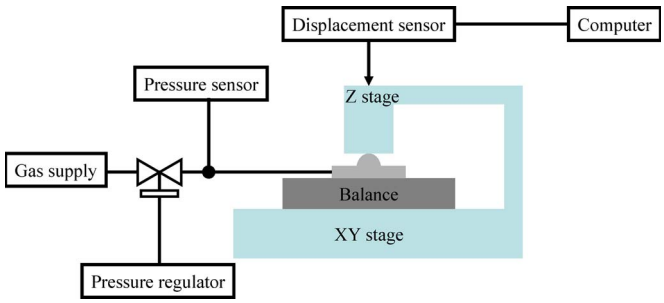

Fig. 11. Diagram of force measurement.

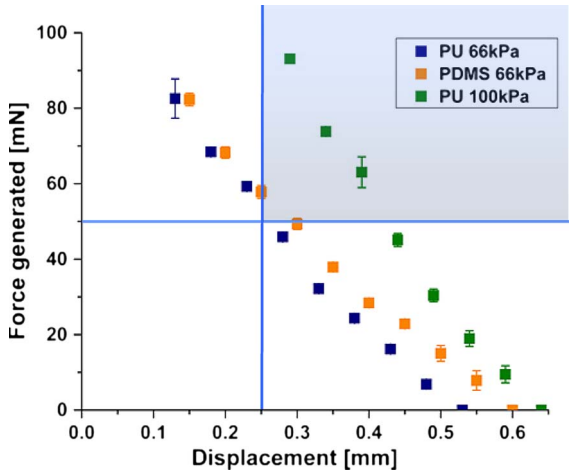

Fig. 12. Force generated by an actuated PU Braille dot and an actuated PDMS Braille dot.

curve represents the stiffness of the microbubble actuator. The stiffness of the PU-based microbubble actuator increases with the actuation pressure. Under the same applied pressure, the PDMS-based microbubble actuator maintains a higher displacement than the PU-based ones at the same force level.

For practical Braille cell operation, the force needs to exceed 50 mN, and the displacement needs to exceed 0.25 mm. This region is highlighted in Fig. 12. The performance of PDMS-based Braille cells falls within this region when the applied pressure is at 66 kPa with a narrow practical range between 0.25- and 0.3-mm displacements. When the applied pressure exceeds 66 kPa, Both PU and PDMS-based Braille cells fall within the practical operation range.

D. Mechanical Bandwidth

To test the mechanical bandwidth of a Braille dot, a steady pressure of 100 kPa was applied to the inlet of the Braille dot. A series of sine-wave inputs of varying frequencies was applied to the valve controlling a single Braille dot. The sinusoidal input was modulated by the binary transfer function of the mechanical valve and adjusted to a 50% pulsewidth-modulation duty cycle at the frequency of interest, producing a pseudo-square-wave pressure pulse to the dot, with the minimum being the atmospheric pressure and the maximum being 100 kPa over that. The maximum and minimum displacements of the Braille dot as a function of excitation frequency in the range of 0.2–200 Hz were measured. The relative (i.e., the peak-to-peak

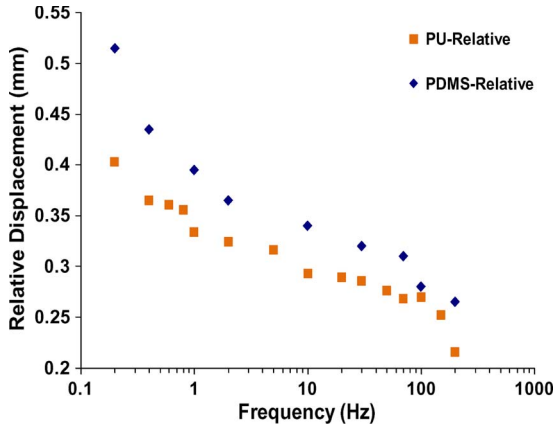

Fig. 13. Frequency response of Braille dots.

difference between maximum and minimum) displacement is plotted against frequency in Fig. 13.

For the PU-based Braille dot, at an actuation frequency of 30 Hz, the peak-to-peak displacement magnitude falls to approximately 70% of that at 0.2 Hz. At a 150-Hz excitation frequency, the peak-to-peak displacement is approximately 0.25 mm, which still meets the minimum requirement of a few micrometers for a dynamic Braille display [19]. Furthermore, even at 200 Hz, the displacement of 0.22 mm is still more than 50% of the maximum displacement of 0.403 mm. The PDMS-based Braille dot has a higher initial peak-to-peak displacement, which decays quickly when frequency increases. At 30 Hz, the peak-to-peak displacement is about 60% of that at 0.2 Hz. Because of the high initial peak-to-peak displacement, even at 200 Hz, the peak-to-peak displacement is 0.265, which is more than 50% of the maximum displacement of 0.515 and higher than that of the PU Braille dot. The high-frequency performance of these RBD cells suggests the feasibility of their application to a vibratory tactile display, because according to physiological studies, 200–300 Hz is the most sensitive range for vibration sensing by human skin [25].

The relative displacements of a PDMS- and a PU-based Braille dot measured at 0.2 Hz are compared in Fig. 14. At the same maximum displacement, the PDMS-based Braille dot has a higher relative displacement than the PU-based Braille dot across the entire pressure range. This means that the minimum displacement of the PDMS-based Braille cell is always lower than that of the PU-based Braille dot, which indicates that PDMS recovers more than PU does during the deflation of the dot, i.e., PDMS has lower hysteresis than PU. A detailed discussion on hysteresis is provided later in this paper.

Several factors that may potentially contribute to the dynamic response of the Braille dot are analyzed hereinafter.

1) Valve Response: The valve used has a response time of 3 ms. At the maximum testing frequency of 200 Hz, the microvalve opens and closes every 5 ms. Because the response time is shorter than the cycle, the size of the microvalve orifice can be maintained up to a driving frequency of at least 200 Hz. Therefore, valve response is unlikely a contributing factor.

2) Filling Time: A Braille cell can be analogized to an RC circuit. The microbubble actuator of the Braille dot acts as the capacitor being charged through a resistor, which, in

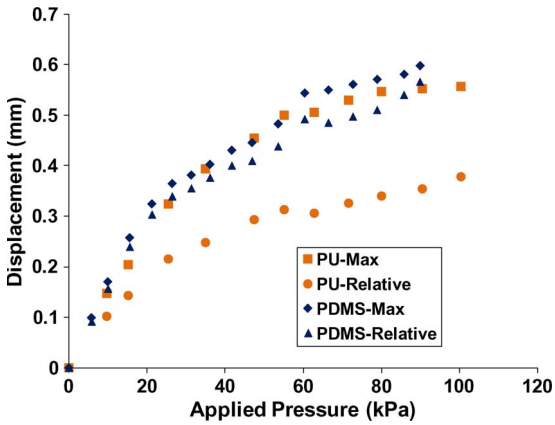

Fig. 14. Relative displacements of a PU Braille dot and a PDMS Braille dot at 0.2 Hz.

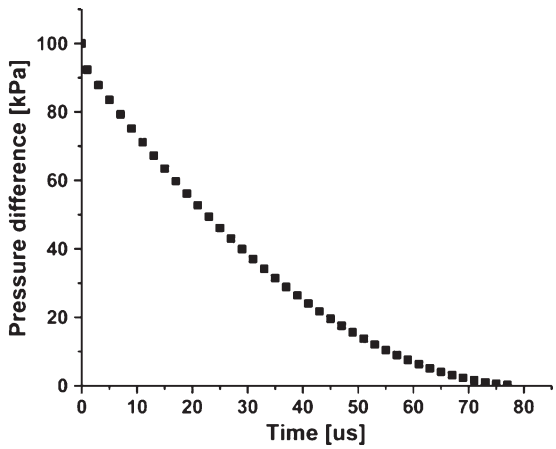

Fig. 15. Pressure difference between gas supply pressure and actuator pressure as a function of time after the valve is open.

this case, the fluid resistance. In an RC circuit, the RC time constant measures the time required to charge the capacitor to a certain percent of full charge. In a microbubble actuator, we can similarly calculate the time required to fully "charge" the bubble (i.e., to have the pressure inside the bubble reach the level of applied pressure) by applying the ideal gas law, the Bernoulli equation, and the mass conservation equation.

At any small time variation t_i, the ideal gas law is

$$PV = nRT \quad \text{or} \quad P = \rho \frac{R}{m} T \tag{1}$$

where P is pressure, V is the volume of the actuator, n is the number of moles of gas, R is the ideal gas constant, T is the absolute temperature, ρ is the density of the gas, and m is the mass of the gas.

Bernoulli's equation can be expressed as

$$P_s - P_i = \frac{1}{2} \rho_i v^2 \tag{2}$$

where P_s is the pressure of the gas supply, P_i is the pressure in the actuator at any time t_i, ρ_i is the density of the gas in the actuator at any time t_i, and v is the gas velocity.

By mass conservation

$$\rho_i V = (\rho_s v A) \Delta t + \rho_{i-\Delta t} V \tag{3}$$

where A, the cross-sectional area normal to the flow direction, is 1.54×10^{-6} m^2 based on a flow path diameter of 1.4 mm, $P_s = 2 \times 10^5$ Pa, and $\rho_s = 2.45$ kg/m^3.

The initial conditions are at time t_0, $P_0 = 1 \times 10^5$ Pa, $V = 4 \times 10^{-8}$ m^3, and $\rho_0 = 1.225$ kg/m^3.

Based on the calculation, the difference between the pressure at the valve inlet and the pressure inside the actuator $(P_s - P_i)$, which is plotted against time, is shown in Fig. 15. Because the pressure difference reaches zero at 77 μs, a time much shorter than the 5-ms valve open and close time at a testing frequency of 200 Hz, the filling time is unlikely a contributing factor either.

3) Viscoelastic Hysteresis: In cyclic testing, the relaxation (deflation) of the microbubble actuator has been observed to be slower than the inflation. Therefore, the peak-to-peak displacement decreases as the cycling frequency increases, even at very low frequency range. The calculation results in the previous section support the theory that the depressurization time (i.e., the time required for the pressure inside the Braille dot to be reduced to atmospheric pressure) is the same as the pressurization time because the volume, the orifice, and the pressure difference are identical in both cases. The time scale for the depressurizing time is too small to account for the observed slow relaxation. A major asymmetry between inflation and deflation may be the mechanical strain of the polymer composite of the endoskeletal microbubble itself. During pressurization, stresses are induced in the polymer multilayer; during depressurization, the polymer recovers from these stresses. It was known, from the quasi-static inflation and deflation measurements detailed previously [18], that the endoskeletal microbubble can exhibit a viscoelastic hysteresis. The effect of the viscoelastic hysteresis on the observed pressurization asymmetry was thus investigated.

The recovery of a viscoelastic deformed material consists of two stages. The first stage is the fast elastic recovery from the majority of the strain, which is associated with the relaxation of the soft segments of the macromolecules. The second stage is a slow recovery ascribed to viscoelastic relaxation of the rigid chain segments of the macromolecules. The second relaxation time can be extremely long, depending on the material and the time history of the creep development, although given enough time, a viscoelastic deformed elastomer material can recover almost completely (to 97%–98%) [26]. In the quasi-static inflation and deflation cycle of the microbubble actuator at 1 Hz, the recovery time constant appears to be on the order of 1 s. In a previously reported work on an artificial hair cell (AHC) sensor made from PU elastomer, bending tests were conducted on high-aspect-ratio PU elastomer pillars AHC [27]. The recovery time for the bent pillar was on the order of 100 ms upon large bending, and would decrease with the decrease of pillar length. The creep–recovery time constant, as one of the viscoelastic responses of elastomeric materials, is highly dependent on the type of strain, the level of stress and strain, and the strain rate. It is not practical to compare two sets of time constants with different types of strain, strain levels, or strain rates. However, qualitatively, the behavior of the microbubble actuator appears to be consistent with that of the PU AHC. The

longer recovery time constant was due to the larger strain and repetitive stress load that the microbubble actuator experienced. Therefore, the dynamic response of the microbubble actuator may be explained by the viscoelastic nature of the material rather than the device and the apparatus used.

During dynamic operation of the microbubble actuator, higher operating frequency allows less recovery time. This is why the amplitude of peak-to-peak displacement decreases with the increase of operating frequency. However, this slow recovery in any case does not affect the performance of the RBD because the collapsing bubble is not pressurized and thus does not generate any force that a user can feel.

E. Pneumatic Power Consumption

Truly portable pneumatic Braille displays require onboard storage of pressurized gas. Based on the current design, 1 mL of 10-atm compressed air can sustain 24 min of Braille reading at a 5-Hz frequency for a single Braille cell containing six Braille dots.

The volume of a Braille dot was calculated by the following procedure. A microscopic cross-sectional image of an actuated Braille dot was taken at a certain applied pressure. The image was then imported to a 3-D CAD software (Solidworks 2007). A cross-sectional profile was replicated by drawing a line along the image. With the revolving function of the software, a 3-D profile of the actuated Braille dot was reconstructed. The volume information of the Braille dot was obtained by using the mass property analyzing function. It was found that an actuated Braille dot has a volume of 0.46 mm^3 at a 100-kPa applied pressure. We assume that, at any time, there are three Braille dots inflated and three deflated. The volume flow in the Braille cell in 1 s is $0.46 \times 3 = 1.38$ mm^3/s. With a total estimated volume of 10^4-mm^3 air supply, the sustaining time is $10^4/1.38/5 = 1450$ s $= 24$ min.

F. Lifetime

As an actuator for an RBD or for a vibrational tactile display, the microbubble actuator is subjected to dynamic instead of static load. The magnitude of the stress in the microbubble actuator varies with time. Thus, static stress theory does not apply. Under these periodically varying stress conditions, failure could occur well below the yield point of the material. The stress level at which failure occurs would decrease with increasing stress cycles. The stress corresponding to the point of failure for a given number of cycles is known as the "fatigue strength."

The lifetime of a microfabricated device is typically evaluated experimentally. To test the long-term stability and lifetime of the device, a randomly picked PU Braille dot was operated at 60 kPa and a refresh rate of 10 Hz. A laser displacement sensor was used to record the displacement over time. The maximum, minimum, and relative displacements of the Braille dot are shown in Fig. 16. After 33.8 h of operation, the parylene layer failed, as evidenced by the shape of endoskeletal microbubble changing into a hyperinflated balloon, which was an indication that the skeleton lost its sustaining function.

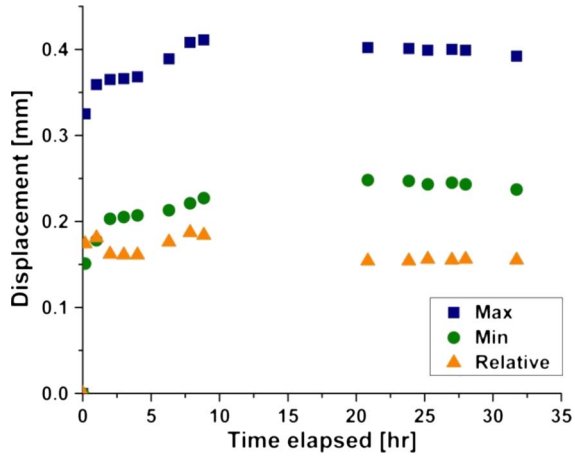

Fig. 16. Long-term actuation stability of the Braille dot.

The tested Braille dot showed a lifetime of 1 216 800 actuations at 10-Hz actuation frequency. The world's best selling book, the New Testament, has a word count of 181 253 and a letter count of 838 380. The tested Braille dot could have sustained the nonstop reading of the New Testament.

During the real operation of a Braille display, the refresh rate is typically slower than 10 Hz, depending on how many cells the display has. Because small variation in operating frequency would not significantly affect the lifetime of polymer materials, the microbubble Braille dot can be operated at 1 Hz for more than 300 h. On the other hand, Braille display is not a device that is usually operated continuously over a long period of time.

To improve the lifetime of the microbubble actuator, it is necessary to identify and reduce detrimental stress factors that influence the fatigue strength of the parylene corrugated diaphragm. The stress concentration at sharp corrugation corners has been identified as the dominant factor. Also, because the diaphragm is made from a micromold, any defects in the micromold may cause potential variation in the parylene thickness, which leads to potential stress concentration points. Both problems can be solved, entirely or partially, by optimizing the fabrication process. For example, a reflow step can be added after the fabrication of the micromold in order to round the sharp corners. The reflow step also helps to improve the smoothness of the micromold. In real-life applications, a fixed usage life can be designated, after which the user is instructed to replace the microbubble actuator layer with a new one.

V. Conclusion

A 2 × 3 pneumatic microbubble actuator array based on modification of a previous design has been successfully fabricated and integrated with a manifold and microvalve array. The modified design enables the microbubble actuator to possess the desired properties in spatial resolution, minimum displacement, minimum force, power consumption, and comfort in operation. In addition, the microbubble actuator can provide both static display and vibratory tactile sensations up to 200 Hz. The strong hysteresis of the microbubble actuator can be resolved by replacing PU elastomer with PDMS elastomer. Both PU- and PDMS-based Braille cells demonstrate satisfactory properties

against the static and vibrational tactile display requirements. The lifetime of the microbubble tactile actuator is approximately 1.2 million cycles. The design of the Braille cell is scalable with respect to the number of dots, and the fabrication remains simple even on a large scale. The device has also been designed to meet the criteria of lightweight and compactness to facilitate portable operation.

ACKNOWLEDGMENT

The authors would like to thank R. Shafer of the Georgia Tech Microsensor and Microactuator Group for his assistance on experiments.

REFERENCES

[1] J. S. Lee and S. Lucyszyn, "A micromachined refreshable Braille cell," *J. Microelectromech. Syst.*, vol. 14, no. 4, pp. 673–682, Aug. 2005.

[2] H. Zhu and W. Book, "Practical structure design and control for digital clay," in *Proc. ASME Int. Mech. Eng. Congr. Expos.*, 2004, pp. 1051–1058.

[3] C. Youngblut, R. E. Johnston, S. H. Nash, R. A. Wienclaw, and C. A. Will, Review of virtual environment interface technology, Inst. Defense Anal., Alexandria, VA, IDA Paper P-3186. [Online]. Available: http://handle.dtic.mil/100.2/ADA314134

[4] M. Benali-Khoudja, M. Hafez, J. M. Alexandre, A. A. K. A. Kheddar, and V. A. M. V. Moreau, "VITAL: A new low-cost vibro-tactile display system," in *Proc. IEEE Int. Conf. Robot. Autom.*, 2004, vol. 1, pp. 721–726.

[5] M. Konyo and S. Todokoro, "Artificial tactile feel display using EAP actuator," *Worldwide ElectroActive Polymers, Artificial Muscles*, vol. 2, no. 1, pp. 1–16, 2000.

[6] X. Wu, H. Zhu, S.-H. Kim, and M. G. Allen, "A portable pneumatically-actuated refreshable Braille cell," in *Proc. TRANSDUCERS*, 2007, pp. 825–828.

[7] A. Bowles, A. Rahman, T. Jarman, P. Morris, and J. Gore, "A new technology for high density actuator arrays," in *Proc. Smart Struct. Mater.—Smart Structures Integrated Systems*, 2005, pp. 680–689.

[8] Y. Ikei, K. Wakamatsu, and S. Fukuda, "Vibratory tactile display of image-based textures," *Comput. Graph. Appl.*, vol. 17, no. 6, pp. 53–61, Nov. 1997.

[9] R. D. Howe, D. A. Kontarinis, and W. J. Peine, "Shape memory alloy actuator controller design for tactile displays," in *Proc. 34th IEEE Conf. Decision Control*, 1995, vol. 4, pp. 3540–3544.

[10] P. M. Taylor, A. Moser, and A. Creed, "A sixty-four element tactile display using shape memory alloy wires," *Displays*, vol. 18, no. 3, pp. 163–168, May 1998.

[11] M. Jungmann and H. F. Schlaak, "Electrostatic actuators with elastic dielectric for use on tactile displays," in *Proc. 8th Int. Conf. New Actuators, Actuator*, 2002, pp. 391–394.

[12] F. Vidal-Verdú and R. Navas-González, "A thermopneumatic approach for tactile displays," in *Proc. IEEE Conf. Mechatron.*, 2004, pp. 395–399.

[13] T. Nara, M. Takasaki, T. Maeda, T. Higuchi, S. Ando, and S. Tachi, "Surface Acoustic Wave (SAW) tactile display based on properties of mechanoreceptors," in *Proc. IEEE Virtual Reality*, 2001, pp. 13–20.

[14] Y. Kato, T. Sekitani, M. Takamiya, M. Doi, K. Asaka, T. Sakurai, and T. Someya, "Sheet-type Braille displays by integrating organic field-effect transistors and polymeric actuators," *IEEE Trans. Electron Devices*, vol. 54, no. 2, pp. 202–209, Feb. 2007.

[15] S. Ukai, T. Imamura, M. Shikida, and K. Sato, "Bubble driven arrayed actuator device for a tactile display," in *Proc. TRANSDUCERS*, 2007, pp. 2171–2174.

[16] L. Yobas, M. A. Huff, F. J. Lisy, and D. M. Durand, "A novel bulk micromachined electrostatic microvalve with a curved-compliant structure applicable for a pneumatic tactile display," *J. Microelectromech. Syst.*, vol. 10, no. 2, pp. 187–196, Jun. 2001.

[17] I. Müller and P. P. Strehlow, *Rubber and Rubber Balloons: Paradigms of Thermodynamics*. New York: Springer-Verlag, 2004.

[18] X. Wu, G. Yuan, Y. K. Yoon, and M. G. Allen, "Kinematically stabilized microbubble actuator arrays," *J. Microelectromech. Syst.*, vol. 17, no. 1, pp. 124–132, Feb. 2008.

[19] S. A. Wall and S. Brewster, "Sensory substitution using tactile pin arrays: Human factors, technology and applications," *Signal Process.*, vol. 86, no. 12, pp. 3674–3695, Dec. 2006.

[20] G. Moy, C. Wagner, and R. S. Fearing, "A compliant tactile display for teletaction," in *Proc. IEEE Int. Conf. Robot. Autom.*, 2000, vol. 4, pp. 3409–3415.

[21] G. E. Legge, C. M. Madison, and J. S. Mansfield, "Measuring Braille reading speed with the MNREAD test," *Vis. Impairment Res.*, vol. 1, no. 3, pp. 131–145, Jan. 1999.

[22] K. Takahata and Y. Gianchandani, "A micromachined capacitive pressure sensor using a cavity-less structure with bulk-metal/elastomer layers and its wireless telemetry application," *Sensors*, vol. 8, no. 4, pp. 2317–2330, Apr. 2008.

[23] H. J. Qi and M. C. Boyce, "Stress–strain behavior of thermoplastic polyurethanes," *Mech. Mater.*, vol. 37, no. 8, pp. 817–839, 2005.

[24] J. M. Loomis, "On the tangibility of letters and Braille," *Percept. Psychophys.*, vol. 29, no. 1, pp. 37–46, Jan. 1981.

[25] R. Verrillo, A. Fraioli, and R. Smith, "Sensation magnitude of vibrotactile stimuli," *Attention, Percept., Psychophys.*, vol. 6, no. 6, pp. 366–372, Nov. 1969.

[26] M. van der Schuur, E. van der Heide, J. Feijen, and R. J. Gaymans, "Elastic behavior of flexible polyether (urethane-urea) foam materials," *Polymer*, vol. 45, no. 8, pp. 2721–2727, 2004.

[27] J. M. Engel, J. Chen, C. Liu, and D. Bullen, "Polyurethane rubber all-polymer artificial hair cell sensor," *J. Microelectromech. Syst.*, vol. 15, no. 4, pp. 729–736, Aug. 2006.

Xiaosong (Sharon) Wu received the Ph.D. degree in polymer, textile, and fiber engineering from the Georgia Institute of Technology, Atlanta, in 2008.

Since then, she has been a Senior Research Engineer with The Dow Chemical Company, Midland, MI. She has developed an expertise in both her academic and industrial careers in polymer micro-engineering, conceptual and mechanical design and analysis on polymer microelectromechanical systems (MEMS), characterization of the physical and chemical properties of elastomeric polymers, and exploring new processes and methods to produce unique structures with differentiated properties. She is the author or coauthor of 11 refereed journal publications, four patent applications, and 15 conference proceeding papers.

Seong-Hyok Kim, photograph and biography not available at the time of publication.

Haihong Zhu, photograph and biography not available at the time of publication.

Chang-Hyeon Ji received the B.S. and M.S. degrees in electrical engineering and the Ph.D. degree in electrical engineering and computer science from Seoul National University, Seoul, Korea, in 1995, 1997, and 2001, respectively.

His doctoral dissertation concerned the design, fabrication, and testing of electromagnetic micromirrors for microphotonic applications. He was with the LG Electronics Institute of Technology, Seoul, from 2001 to 2006 as a Senior and Chief Research Engineer, where he developed microactuators for various types of applications, including optical communication and raster scanning laser display system. From 2006 to 2011, he was a Postdoctoral Fellow with the Georgia Institute of Technology, Atlanta, where he researched micro power generators and energy scavengers, micromachined components and through-wafer interconnection technology for integrated power electronics, and microfabricated components for wireless power transfer and energy storage. In 2011, he joined the faculty of the Department of Electronics Engineering, Ewha Womans University, Seoul, where he is currently an Associate Professor. His current research interests include power microelectromechanical systems (MEMS), bio-MEMS, and nanofabrication technology.

Mark G. Allen (M'88–SM'04–F'11) received the B.A. degree in chemistry, the B.S.E. degree in chemical engineering, and the B.S.E. degree in electrical engineering from the University of Pennsylvania, Philadelphia, and the S.M. and Ph.D. degrees from the Massachusetts Institute of Technology, Cambridge.

In 1989, he joined the faculty of the School of Electrical and Computer Engineering, Georgia Institute of Technology, Atlanta, where he currently holds the rank of Regents' Professor and the J.M. Pettit Professorship in Microelectronics, as well as a joint appointment in the School of Chemical and Biomolecular Engineering. His research interests are in the development and application of new micro- and nanofabrication technologies, as well as microelectromechanical systems.

Dr. Allen is the Editor-in-Chief of the *Journal of Micromechanics and Microengineering* and the previous Co-Chair of the IEEE/American Society of Mechanical Engineering Microelectromechanical Systems Conference.